Direct observation of Ga-rich microdomains in crack-free AlGaN grown on patterned GaN/sapphire substrates

T. Riemann[a] and J. Christen
Otto-von-Guericke-University Magdeburg, P.O. Box 4120, 39016 Magdeburg, Germany

A. Kaschner, A. Laades, A. Hoffmann, and C. Thomsen
Technical University Berlin, Hardenbergstr. 36, 10623 Berlin, Germany

M. Iwaya, S. Kamiyama, H. Amano, and I. Akasaki
Meijo University, 1-501 Shiogamaguchi, Tempaku-ku, Nagoya 468-8502, Japan

(Received 9 November 2001; accepted for publication 21 February 2002)

The strong three-dimensional modulation of the optical and structural properties due to the self-organized formation of Ga-rich AlGaN microdomains is directly imaged by spectrally and spatially resolved cathodoluminescence microscopy. The 5-μm-thick, crack-free AlGaN was grown on patterned GaN/sapphire templates periodically structured into trenches and terraces. During initial AlGaN overgrowth, the modulation of the local AlGaN stochiometry results in marble-like striations of Ga accumulation clearly reflecting the pattern periodicity. In contrast, after subsequent overgrowth, a homogeneous emission wavelength, i.e., a homogeneous aluminum content, is found near the sample surface. However, the strong rise of quantum efficiency directly above the trenches indicates a drastic improvement of material quality. © *2002 American Institute of Physics.*
[DOI: 10.1063/1.1473703]

For efficient performance of GaN-based electronic devices as well as for optoelectronic devices operating in the ultraviolet region, high crystalline quality and chemical homogeneity of AlGaN is mandatory. However, AlGaN is susceptible both to fluctuations of the Al content and to extended structural defects including microcracks. Masking techniques like epitaxial lateral overgrowth or pendeo epitaxy, which lead to a strong reduction of dislocation density in GaN, are not appropriate for AlGaN because the Al alloys also nucleate on the mask materials. Recently, growth on patterned substrates has proven favorable to achieve thick, crack-free AlGaN layers.[1–3] In this letter, the impact of this approach on the microscopic optical and structural AlGaN properties is investigated by cathodoluminescence microscopy (CL) and micro-Raman spectroscopy (μ-Raman). Details of our low temperature CL setup, e.g., yielding CL intensity images (CLI) and CL wavelength images (CLWI), as well as the μ-Raman technique are given in Refs. 4–6.

The sample under study was grown by metal organic vapor phase epitaxy using a (0001) sapphire substrate.[2] First, a 4 μm GaN layer was grown on low temperature (LT)-AlN/sapphire and subsequently structured into a periodic grid of trenches and terraces along $\langle 1\underline{1}00\rangle$. Prior to the final AlGaN ($[\mathrm{Al}]=0.19$) deposition, this patterned template was again overgrown with a LT-AlN interlayer, as schematically indicated in Fig. 1(a).

The scanning electron microscopy (SEM) image Fig. 1(b) shows a cross-sectional view of the sample perpendicular to the trench direction, i.e., perpendicular to $\langle 1\underline{1}00\rangle$. It covers two trenches as marked in Fig. 1(a). The patterned GaN layer and the final AlGaN can be easily distinguished by SEM contrast.

Additional features appearing in the AlGaN layer, e.g., inside the trenches, indicate a spatial modulation of the AlGaN properties. The spectrum Fig. 1(c) represents the CL emission averaged over the whole cross section displayed in Fig. 1(b). While a weak, single peak is found for the luminescence of the patterned GaN layer, the dominant AlGaN emission clearly consists of three main spectral contributions labeled A, B, and C, ranging from 300 to almost 350 nm. Using CL imaging, each of these components can be unambiguously assigned to a specific type of AlGaN microdomains.

To achieve a complete characterization of the complex, three-dimensional domain geometries, cross-sectional CL scans in different orientations were performed in addition to plan view CL mappings. The various scan orientations are schematically illustrated in Fig. 2. As a result, we present a set of CLWIs in Fig. 3, mapping the AlGaN emission wavelength exactly using these scan orientations. For a better understanding, the individual CLWIs (a)–(f) of Fig. 3 are arranged according to the annotations (a)–(f) in Fig. 2.

Starting with Fig. 3(e) which is recorded on the frontal $\{1\underline{1}00\}$ cross section, the $\{0001\}$ plan view orientation is flipped vertically by 90° for Fig. 3(b), while the side cross

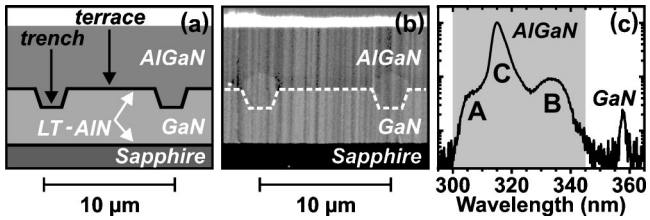

FIG. 1. (a) Schematic sample structure, (b) cross-sectional SEM image perpendicular to the trench direction, and (c) CL spectrum averaging the emission of the area shown in (b).

[a]Electronic mail: till.riemann@student.uni-magdeburg.de

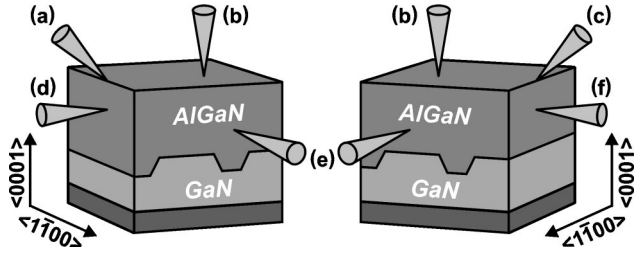

FIG. 2. Schematic illustration of the CL scan orientations used for the set of CL wavelength images in Figs. 3(a)–3(f).

sections $\{\underline{11}20\}$ in Fig. 3(d) and $\{11\underline{2}0\}$ in Fig. 3(f) are horizontally flipped by 90° to the left and to the right, respectively. For Figs. 3(a) and 3(c) the sample is tilted by 45° enabling the viewing of the {0001} surface together with the $\{\underline{11}20\}$ or the $\{11\underline{2}0\}$ cross sections, respectively.

This way, Fig. 3(d) shows a scan parallel to $\{\underline{11}20\}$, where the cleavage plane runs along the trench center. An analogous area is displayed in the lower part of Fig. 3(a). Because of the tilted scan direction of (a), the sample surface is included in its upper part. For Figs. 3(c) and 3(f), the sample was cleaved along $\{11\underline{2}0\}$. In contrast to (a) and (d), the cleavage plane now follows the terrace center. As in Fig. 3(d), in (f) only the cleaved $\{11\underline{2}0\}$ face is mapped. Again, the tilted view (c) covers the transition to the sample surface similar to (a).

The region of initial AlGaN growth on the terraces (A) in Figs. 3(c), 3(e), and 3(f) emits high-energetic luminescence centered at 305 nm. With advancing vertical growth this domain also expands laterally over the trenches, finally leading to coalescence above the trench centers. Parallel we observe a slight overall redshift of the peak position, indicating a vertical gradient of aluminum content.

In strong contrast, the domain of initial AlGaN growth inside the trenches (B) [Figs. 3(a), 3(d), and 3(e)] is completely dominated by low-energetic luminescence near 335 nm, indicating a strong Ga accumulation. The lateral size of this domain B is limited by the trench width. The self-organized lateral expansion of A eventually inhibits further vertical growth of B, leading to the pentagonal shape in the cross section Fig. 3(e). At the trench bottom we find statistical fluctuations of the peak position, i.e., the local Al concentration, for the very first stage of growth. AlGaN growth on the trench side facets is initially accompanied by emission red shifted up to 340 nm. All domains B exhibit a strong redshift of the emission wavelength from the outer trench edges towards the domain top, indicating a gradual Ga accumulation during growth.

While A and B clearly reflect the template patterning, the emission wavelength of the final domain C is almost independent of the lateral sampling position. Following the self-organized transition from domains A and B to C, we find an average emission wavelength of 315 nm up to the sample surface. However, C exhibits strong vertical modulations of this average emission energy, appearing as curved lines of redshifted luminescence, i.e., reduced [Al], in Fig. 2(e). The cross-sectional CLWIs parallel to $\{11\underline{2}0\}$ reveal the real, three-dimensional, marble-like geometry of these modulations. In Figs. 3(d) and 3(f), these [Al] modulations inside C are visualized by tilted, parallel lines of redshifted luminescence, running straight to the sample surface.

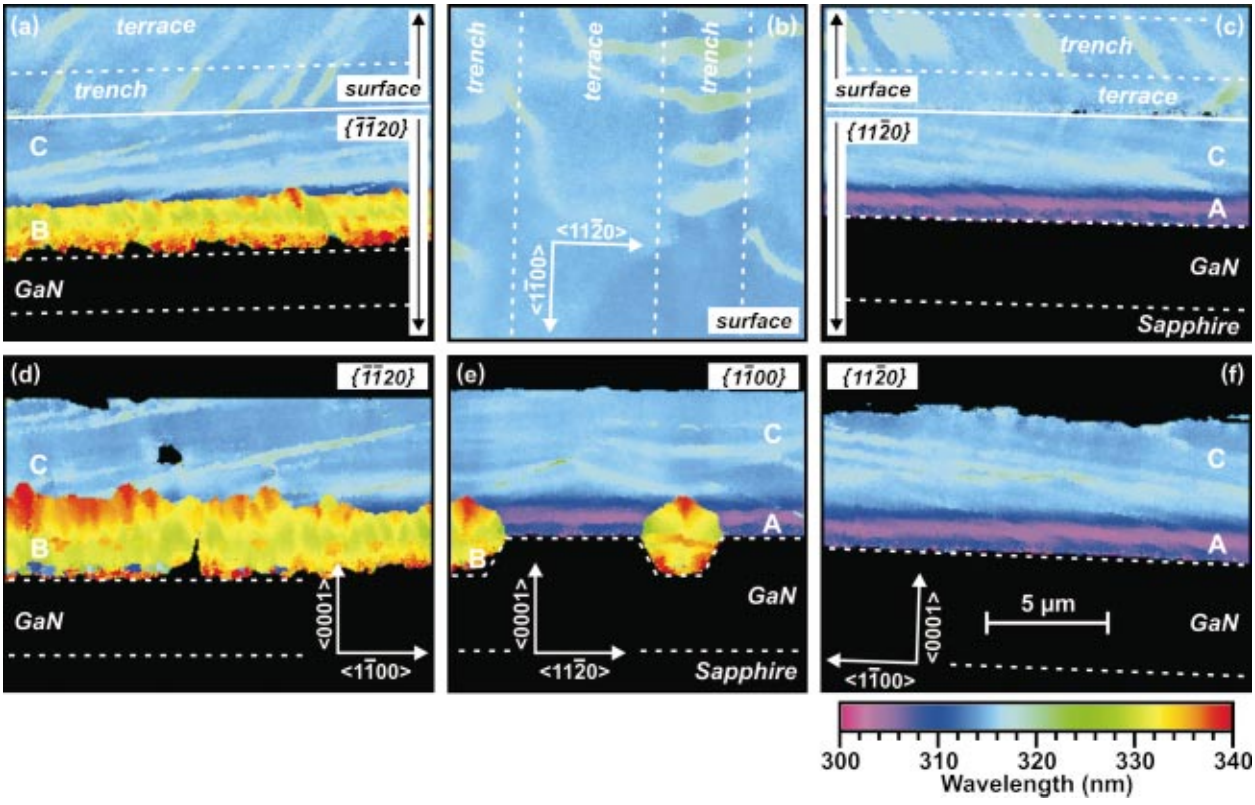

FIG. 3. (Color) Visualization of the AlGaN microdomain structure by cross-sectional and plan view mappings of the CL emission wavelength. In the cross sections (d), (e), and (f) the $\{\underline{11}20\}$, $\{1\underline{1}00\}$, and $\{11\underline{2}0\}$ lattice planes are scanned, respectively. The plan view scan (b) images the {0001} sample surface. The scans (a) and (c) are taken under an angle of 45° showing the {0001} surface together with either the $\{\underline{11}20\}$ or $\{11\underline{2}0\}$ cross sections.

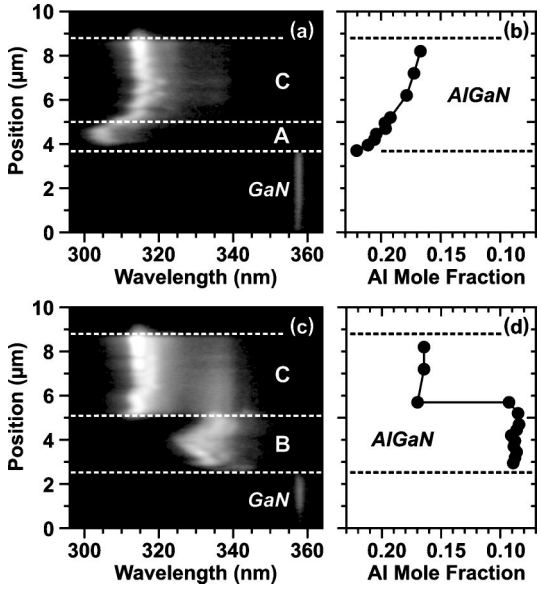

FIG. 4. Evolution of CL emission and aluminum content along ⟨0001⟩: (a) and (b) above terrace; (c) and (d) above trench, respectively. [In the CL linescans Figs. 3(a) and 3(c) bright contrast means high CL intensity.]

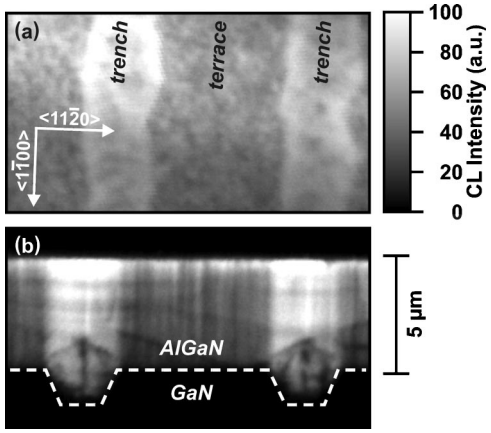

FIG. 5. Modulation of AlGaN quantum efficiency with pattern periodicity: CL intensity images integrating the AlGaN emission (300–340 nm) of the (a) as-grown sample surface, and (b) the corresponding cross section perpendicular to the trench direction.

Sporadic defects in the otherwise homogeneous surface emission energy, as visible in Fig. 3(b), appear exactly where the planes of the marbled structure penetrate the sample surface. This effect is illustrated by the CLWIs Figs. 3(a) and 3(c), both showing cross-sectional and surface emission of domain C at once.

Using μ-Raman to directly determine the local [Al], we find a perfect agreement with the CL results. Here, the Al concentration is derived from the A_1(TO) phonon energy.[7–10] In Fig. 4 we compare CL linescans along ⟨0001⟩ with the corresponding μ-Raman measurements. The CL linescan Fig. 4(a) crosses the terrace center. Above the GaN layer, it first shows the emission of A at 305 nm before inside C the emission shifts to 315 nm. The same way, the μ-Raman line scan Fig. 4(b) proves $[\mathrm{Al}]=0.22$ directly above the terraces, while $[\mathrm{Al}]=0.17$ is reached underneath the sample surface. In contrast, in Fig. 4(c), which corresponds to the trench center, the AlGaN emission starts at 335 nm inside B, exactly where μ-Raman evidences $[\mathrm{Al}]=0.09$ in Fig. 3(d). Following the abrupt transition to C, also above the trenches we find $[\mathrm{Al}]=0.17$ consistent with the CL emission wavelength near 335 nm, i.e., the identical values as for the upper region above the terraces in (a) and (b).

While the influence of the template patterning on the surface emission energy is weak, we observe a drastic impact on quantum efficiency. Figure 5 shows CLIs, integrating the AlGaN emission from 300 to 340 nm. The cross-sectional CLI Fig. 5(b) visualizes a strong increase of CL intensity above the trenches. Also when mapping the sample surface, the trench positions are still revealed. The dark spots appearing in the plan-view CLI Fig. 5(a) directly visualize the drop of quantum efficiency around dislocations. Above the trenches we find a strongly reduced density of these dark spots, indicating a drastic improvement of crystalline quality in these regions.

In summary, AlGaN growth ($[\mathrm{Al}]=0.19$) on patterned GaN/sapphire substrates was found to lead to the self-organized formation of marble-like striations of Ga-rich microdomains. A detailed analysis of the generic domain properties, i.e., the luminescence characteristics and aluminum content, was achieved by combining CL microscopy and μ-Raman spectroscopy: The onset of initial AlGaN growth on the planar terrace regions results in luminescence at 305 nm and an Al concentration of $[\mathrm{Al}]=0.22$. In contrast, self-limited AlGaN growth inside the trenches leads to an emission band centered at 335 nm in agreement with $[\mathrm{Al}]=0.09$. After a self-organized transition following 2 μm AlGaN deposition, an emission wavelength around 315 nm and an average Al concentration of 0.17 are observed independent of the lateral position. All AlGaN microdomains additionally show specific modulations of their average [Al]. While at the surface the emission energy exhibits a homogeneous distribution with sporadic defects, above the trenches a drastic reduction of dislocation density is evidenced.

This work is supported by the Deutsche Forschungsgemeinschaft Contract Nos. CH 87/4-2 and THO 662/4-2.

[1] M. Yano, T. Detchprohm, R. Nakamura, S. Sano, S. Mochizuki, T. Nakamura, H. Amano, and I. Akasaki, IPAP Conf. Series **1**, 292 (2000).
[2] M. Iwaya, R. Nakamura, S. Terao, T. Ukai, S. Kamiyama, H. Amano, and I. Akasaki, IPAP Conf. Series **1**, 833 (2000).
[3] T. Detchprohm, M. Yano, S. Sano, R. Nakamura, S. Mochizuki, T. Nakamura, H. Amano, and I. Akasaki, Jpn. J. Appl. Phys., Part 2 **40**, L16 (2001).
[4] J. Christen, M. Grundmann, and D. Bimberg, J. Vac. Sci. Technol. B **9**, 2358 (1991); J. Christen and T. Riemann, Phys. Status Solidi B **228**, 419 (2001).
[5] F. Bertram, T. Riemann, J. Christen, A. Kaschner, A. Hoffmann, C. Thomsen, K. Hiramatsu, T. Shibata, and N. Sawaki, Appl. Phys. Lett. **74**, 359 (1998).
[6] A. Kaschner, A. Hoffmann, C. Thomsen, F. Bertram, T. Riemann, J. Christen, K. Hiramatsu, H. Sone, and N. Sawaki, Appl. Phys. Lett. **76**, 3418 (2000).
[7] H. Siegle, Ph.D. thesis, Technical University Berlin, Germany, 1998.
[8] A. Cros, H. Angerer, O. Ambacher, M. Stutzmann, R. Höpler, and T. Metzger, Solid State Commun. **104**, 35 (1997).
[9] L. Bergman, M. D. Bremser, W. G. Perry, R. F. Davis, M. Dutta, and R. J. Nernanich, Appl. Phys. Lett. **71**, 2157 (1997).
[10] F. Dernangeot, G. Groenen, J. Frandon, M. A. Renucci, O. Briot, S. Clur, and R. L. Aulornbard, Appl. Phys. Lett. **72**, 2674 (1998).